
Article:
Hart, J., Sonnenwald, F., Stovin, V. et al. (1 more author) (2021) Longitudinal dispersion in unsteady pipe flows. Journal of Hydraulic Engineering, 147 (9). ISSN 0733-9429

https://doi.org/10.1061/(ASCE)HY.1943-7900.0001918

Longitudinal Dispersion in Unsteady Pipe Flows

James Hart, Fred Sonnenwald, Virginia Stovin and Ian Guymer

Abstract

Temporal concentration profiles resulting from an injected pulse of fluorescent tracer were recorded at multiple locations along a pipe during controlled unsteady flow conditions. A linear temporal change in discharge over durations of 5, 10, or 60 s for both accelerating and decelerating flow conditions was studied. Tests were performed for flows that changed within the turbulent range, between Reynolds numbers of 6,500 and 47,000, and for laminar to turbulent flows, between Reynolds numbers of 2,700 and 47,000. Analysis of the data shows the limitations of employing steady-state routing of temporal concentration profiles in unsteady flows. Employing a 'flow weighted time' routing approach, using tracer mean velocity and dispersion coefficients, provides accurate predictions of mixing in unsteady flow. For decelerating flows, longitudinal dispersion coefficients were lower than for the equivalent mean steady discharge. Previously unreported disaggregation of the tracer cloud was observed during all experiments accelerating from laminar to turbulent conditions.

Introduction

It is important to understand the fate of solutes in drinking water supply networks. Examples include disinfectants introduced into the network by the operator, or contaminants that unintentionally find their way into the network. Basha and Malaeb (2007) highlight the importance of including dispersion effects, especially in low velocity pipes. The ability to model the mixing of these solutes, and therefore predict the peak concentration and longitudinal spread at downstream locations, is required to ensure water quality throughout the network.

Water mains and central regions of water supply networks operate under conditions of steady, turbulent flow, where theory derived from Taylor's original analysis (Taylor, 1954) is sufficient to estimate dispersion. However, local regions of the distribution network, where water leaves the main network, often experience much lower discharges, and conditions in these regions have been shown to be turbulent, transitional or even laminar (Buchberger et al., 2003). Furthermore, as discharge is a function of local, intermittent demand, flows can also be highly time varied and do not necessarily hold to the steady flow assumption (Buchberger et al., 2003). The aim of this paper is to experimentally investigate longitudinal dispersion in unsteady flow and to assess the degree to which solute transport routing can be applied and extended to unsteady flows of different acceleration durations.

The fundamental fluid dynamics for unsteady pipe flows have been studied in the laboratory by several authors. Kurokawa and Morikawa (1986) investigated the effect of acceleration and deceleration on pipe flow by measuring temporal velocity profiles at different radial locations using hot wire anemometer. The flow was either accelerated or decelerated between stationary conditions (i.e. Re = 0) and a discharge corresponding to Re = 73,000. A range of acceleration and deceleration durations was investigated. Figure 1, reproduced from Kurokawa and Morikawa (1986) in simplified form, shows the temporal variation in velocity at four radial positions (γ/r), where γ is the distance from the pipe wall and r is the pipe radius. The results from the maximum and minimum acceleration durations studied, 2.5 s and 25 s, are shown in Figure 1a and 1b respectively. As the flow accelerates from stationary conditions, a point of transition can be seen in both time series between the centreline and pipe boundary regions. Around this transition, the central core of the flow ($\gamma/r \geq 0.50$) exhibits a smoother acceleration compared to the flow closer to the pipe

boundary ($y/r < 0.50$). These transitions occur at different times and Reynolds numbers, depending on the acceleration duration, and in both cases the transition velocity is higher than it would be for the transition from laminar to turbulent flow to occur under steady flow conditions. Around the transition there is a rapid temporal change, and spatial differences in velocity of up to 100% were recorded. This period of non-equilibrium will impact on the longitudinal mixing of solutes within the flow.

He and Jackson (2000) measured velocity profiles in turbulent, unsteady pipe flow using a two-component LDA system. For the main test series, they considered fully turbulent flows which were accelerated or decelerated between Reynolds Numbers of 7,000 and 45,200 and considered the effects of acceleration duration on the velocity profile in terms of a dimensionless ramp rate parameter. This parameter allowed the authors to quantify whether the flow was equivalent to fully developed steady flow at each discrete cross-sectional velocity, a case deemed 'pseudo-steady flow'. In the slowest acceleration, with an acceleration duration of 45 s, the velocity profiles showed no difference between measured and predicted steady flow profiles. In contrast, during the early stages of the fastest acceleration, over 5 s, the velocity was measured to be slightly lower than the 'pseudo-steady velocity' values near the pipe centre and slightly higher close to the pipe boundary. The magnitude of these differences was < 10%, much less than differences recorded by Kurokawa and Morikawa (1986).

Greenblatt and Moss (2004) measured velocity profiles, using 1D LDA in transient water pipe flow and considered three acceleration durations, all shorter than the previous studies of Kurokawa and Morikawa (1986) and He and Jackson (2000). The acceleration durations were around 0.5, 1.25 and 2.5 s and for all cases considered, the flow was always turbulent with an initial Reynolds number of 31,000 and a final value of 82,000. Profile parameters exhibited similar qualitative trends to one another when time was scaled with the acceleration duration and this differed from corresponding spatial development of flows subjected to steady streamwise pressure gradients.

In summary, previous studies highlight that, for long acceleration durations, unsteady pipe flow can be approximated by a steady flow model. In contrast, for short acceleration durations, the approximation becomes less accurate. This is most clearly illustrated as the flow accelerates from laminar to fully turbulent in the results from Kurokawa and Morikawa (1986), Figure 1, which show significant discontinuities occurring in the radial velocity profile for a rapid acceleration. Given the effects of flow acceleration on the hydrodynamics, this paper investigates how these impact on solute mixing.

Longitudinal dispersion for steady pipe flow was initially investigated by Taylor (1953, 1954), who showed that after an initial period required for the solute to become cross-sectionally well mixed, the longitudinal distribution of the solute's cross-sectional mean concentration will be Gaussian. Shear dispersion is the result of radial variations of the velocity profile. Initially after injection, shear effects are out of balance with pure advection, which impart considerable skewness to the concentration profile. After an initial period, long enough for the contaminant to experience the complete flow field, a balance is established between the processes of shear dispersion and molecular or turbulent diffusion. Analysis by Chatwin (1970) has shown that the time scale to become cross-sectionally well-mixed is $\approx 0.2r^2/D_m$ where D_m is the molecular diffusion coefficient. This is an order of magnitude greater than that estimated by Taylor (1954). Following the initial period, the variance of the concentration profiles increases linearly with time and the skewness decreases. Through Taylor's analysis, the effects of dispersion in a pipe can be modelled by a gradient diffusion term. The area averaged one-dimensional form of the advection dispersion equation (ADE) used for longitudinal mixing is:

$$\frac{\partial c}{\partial t} + u\frac{\partial c}{\partial x} = D\frac{\partial^2 c}{\partial x^2} \quad (1)$$

where c is concentration, t is time, x is longitudinal distance, u is velocity and D is the longitudinal dispersion coefficient accounting for the mixing processes: molecular and turbulent diffusion and shear dispersion. Assuming an instantaneous injection, Equation 1 can be solved to give the concentration profile downstream in a pipe after a given period of time as:

$$c(x,t) = \frac{M}{A\sqrt{4\pi Dt}} exp\left(-\frac{(x-ut)^2}{4Dt}\right) \quad (2)$$

where A is cross-sectional area and M is mass of injected contaminant (Fischer et al., 1979). This solution provides concentration distributions as a function of longitudinal distance at discrete times, i.e. a snapshot in time, showing the spatial distribution of the contaminant.

Many practical modelling situations require the prediction of a downstream temporal concentration profile, $c(x_2, t)$ from a known upstream profile, $c(x_1, t)$, where x_1 and x_2 are upstream and downstream measurement locations respectively. In such situations, it is possible to use a routing procedure solution to the ADE (Equation 5.20, Fischer et al., 1979). After applying the 'frozen cloud' approximation by substituting $x = ut$, replacing M with the upstream concentration profile and convolving Equation 2 with respect to time, the routing solution to the ADE is:

$$c(x_2,t) = \int_{\gamma=-\infty}^{\infty} \frac{c(x_1,\gamma)u}{\sqrt{4\pi D\bar{t}}} \exp\left[-\frac{u^2(\bar{t}-t+\gamma)^2}{4D\bar{t}}\right] d\gamma \quad (3)$$

where $\bar{t}$ is travel time, the difference in time between the centroids of the upstream and downstream concentration profiles and γ is an integration variable representing time. Equation 3 assumes steady-state conditions and predicts a downstream temporal concentration profile based on a known upstream profile.

Taylor proposed two expressions for the longitudinal dispersion coefficient, one for laminar and another for turbulent pipe flow. Taylor's expression for the dispersion coefficient within laminar flow was derived assuming a parabolic velocity profile, whereas for turbulent flow he assumed a logarithmic velocity profile, typical of highly turbulent flow. Following Taylor's work, as shown in Hart et al. (2016), several other authors recorded data that demonstrated deviation between experimentally obtained dispersion coefficients and Taylor's expression for Reynolds numbers (*Re*) below 20,000. This deviation is due to the increasing significance of the boundary layer for *Re* < 20,000, causing increased longitudinal differential advection that is not accounted for by Taylor's assumption of a logarithmic velocity profile with no boundary layer (Hart et al., 2013).

Whilst Taylor's expression, which assumes the solute to be well mixed and in equilibrium, is valid for laminar flow, Hart et al. (2016) showed that it is not applicable in practice. In laminar flow, where the only radial exchange is that of molecular diffusion, well-mixed conditions can take the order of days or even weeks to develop in standard water distribution-sized pipes. Hart et al. (2016) suggested an alternative approach based on the Residence Time Distribution (RTD) (Danckwerts, 1953). This approach was shown to vastly improve the prediction of the downstream temporal concentration profile for Re < 3,000 at short times from injection.

Romero-Gomez and Choi (2011) provide additional evidence that the standard approach of Taylor can be improved upon in laminar flow systems. For water supply systems, they developed and experimentally verified a direction-dependent approach, giving forwards and backwards dispersion rates. The approach demonstrated an improvement over the conventional formula using various combinations of pipe lengths, tracer injections, mean flow velocities, and solute properties. Piazza et

al. (2020) employed the approach of Romero-Gomez and Choi (2011) within an EPANET water distribution network model to show the importance of diffusive processes when the velocity is low.

Hart et al. (2016) showed that, although Taylor's expression for longitudinal dispersion coefficient for turbulent flow with *Re* < 20,000 was unsuitable, the magnitude of the dispersion coefficient could be corrected to account for the lower Reynolds Number effects. This enabled acceptable predictions of concentration profiles for both transitional and turbulent flow. In the range 3,000 < *Re* < 50,000, Hart et al. (2016) confirmed that D/ud was a function of Reynolds number, and proposed that for their pipe system the longitudinal dispersion coefficient could be estimated from

$$\frac{D}{ud} = 1.17\text{x}10^{9}Re^{-2.5} + 0.41 \quad (4)$$

where d is the pipe diameter.

Residence Time Distribution (RTD) theory (Levenspiel, 1972) introduced the concept of dimensionless time, which is used to remove the effects of flow rate and volume when comparing the mixing responses of different systems under different conditions. Nauman (1969) investigated unsteady mixing processes in stirred tank reactors using RTDs and showed that RTD principles apply to unsteady flow systems, including dimensionless time. Whilst Nauman (1969) used mean flow rate when calculating dimensionless time, Fernandez-Sempere et al. (1995) examined RTDs from an unsteady sewerage system using a dimensionless time parameter, ϕ. This is based on cumulative volume over a constant system volume, where

$$\phi(t) = V^{-1}\int_0^t Q(\gamma)\mathrm{d}\gamma \quad (5)$$

where V is system volume (the volume of water between measurement locations) and Q the flow rate.

For stormwater treatment systems, Werner & Kadlec (1996) investigated the concept of a dimensionless time based on volume in more detail, naming ϕ 'flow weighted time'. They illustrated the differences between RTDs obtained for the same system, depending on injection time in unsteady flow, and showed that these differences were significantly minimised in flow weighted time. Werner & Kadlec (1996) analysed the RTD in flow weighted time concept and showed the RTD to have 0th and 1st moments of 1.0. This is desirable as it shows that the unsteady, or flow weighted time RTD has many of the same statistical properties as the conventional steady RTD confirming the results of Nauman (1969). The flow weighted time concept has since been used to analyse concentrations across a range of unsteady flow problems (Leclerc et al., 2000, Wahl et al., 2012, and Holland et al., 2004).

The aim of the present paper is to extend the application of flow weighted time-based analysis for application to the prediction of longitudinal dispersion in unsteady pipe flows. The work is underpinned by new laboratory data that quantifies longitudinal dispersion in a pipe subjected to unsteady conditions. We propose a new form of the solute transport routing equation based on flow weighted time, and test its application to the laboratory data through the estimation of longitudinal dispersion coefficients from the laboratory data.

Methodology

Experimental Methodology

In water supply networks, a wide range of discharge patterns can be experienced. However, as one of the first studies into the phenomena, this paper will only consider the case of flow accelerated or decelerated at a constant gradient from an initial steady discharge to a final steady discharge.

The experimental results presented here were collected in the same laboratory rig used by Hart et al. (2016). A simplified schematic of the set-up on the 24 mm diameter pipe is provided in Figure 2. During some preliminary tracer tests, multiple concentration peaks were recorded at these instrument locations. Hence, the previous experimental configuration was modified to confirm the profile of the injected tracer cloud by locating an additional Turner Designs Series 10 fluorimeter 0.5 m downstream from the injection point. This is shown in Figure 2. Due to the close proximity of this instrument to the injection location, the peak tracer concentration here was greater than the maximum that could be recorded in some cases.

Unlike the steady flow study described by Hart et al. (2016), this series of experiments was conducted with a linear temporal change in discharge over durations of 5, 10, or 60 s. A schematic of the flow and test conditions is provided in Figure 3. The instantaneous discharge was measured using an electromagnetic flow meter (Siemens Sitrans FM Mago MAG 5100W) and logged at 30 Hz. For each run, an initial steady discharge was set to provide a predefined initial Reynolds number, Re_i and injection (1) made, shown by the left-hand grey shaded area in Figure 3. The discharge was then accelerated, or decelerated (negative acceleration), at a constant rate, to a final discharge and Reynolds number, Re_f, with further tracer injections made during the unsteady discharge. A single injection (Figure 3, injection 2) was made during each of the 5 and 10 s acceleration durations, with two injections (2 & 3) possible during the longest, 60 s acceleration duration. A further injection (4), was made into the final steady discharge. Discharge was controlled by the pump's digital controller on the basis of a pre-set gradient. 1 s duration tracer injections were made using a peristaltic pump at set times within the discharge acceleration.

Accelerating and decelerating flow conditions were investigated under turbulent flow conditions, between Re_i & Re_f values of 6,500 & 47,000 (Tests 1 and 2), and between laminar and turbulent conditions, between Re_i & Re_f values of 2,700 & 47,000 (in Tests 3 and 4). All traces were repeated five times, resulting in 220 individual injections, each recorded by the 7 fluorimeters between 0.5 and 13.05 m downstream. Unfortunately, the fluorimeter positioned 10.98 m downstream of the injection exhibited significant noise in the output and as a result, none of the data from this fluorimeter has been included. In total, eighty individual traces were performed during transient flow conditions from injections 2 and 3, and a summary of the test conditions is provided in Table 1.

Extending the Routing Approach for Unsteady Flow

The standard routing procedure solution to the ADE equation uses distance or time in steady flow conditions, employing the frozen cloud approximation to convert between spatial and temporal variations (Fischer et al., 1979). In unsteady flows, Eulerian measurements of concentration within a system do not exhibit a linear increase in temporal variance with distance, which prevents the use of the frozen cloud approximation for the determination of longitudinal dispersion coefficients. Here, we propose to use flow weighted time (Werner & Kadlec, 1996) to extend the routing procedure solution to the standard ADE and apply it to unsteady flow conditions.

The solute transport routing equation in dimensionless flow weighted time, ϕ, can be derived from the standard solution Equation 2, again using an analogue of the frozen cloud approximation, letting $\phi \simeq x$. By definition, both travel time and velocity (as units travelled per unit time) are 1 in flow weighted time. Thus, as with the solution for Equation 3, after substitution for ϕ, $\bar{t}$, and u, Equation 2 is convolved with the upstream profile and the flow weighted time routing equation is therefore:

$$S(x_2, \phi) = \int_{\gamma-\infty}^{\infty} \frac{S(x_1,\gamma)}{\sqrt{4\pi J}} \exp\left[\frac{(1+\gamma-\phi)^2}{4J}\right] \mathrm{d}\gamma \quad (6)$$

where $S(x_1, \gamma)$and $S(x_2, \phi)$ are the upstream and downstream concentration profiles in flow weighted time, J is the dimensionless flow weighted time dispersion coefficient, and γ is an integration variable representing flow weighted time. Following dimensional analysis J is given as:

$$J = \frac{D}{us} \tag{7}$$

where $s = x_2 - x_1$ is the distance between measurement points. Flow weighted time is an adjusted time-axis where "time is stretched and compressed" (Werner & Kadlec, 1996), and since both u and s affect the travel time, they are appropriate non-dimensionalisation parameters. Although Equation 6 is in dimensionless units of flow weighted time, it otherwise has the same interpretation of the standard routing solution Equation 3. That is, each portion of the upstream profile is advected downstream and spread out . The sum of these downstream components gives the final downstream profile.

Analysis of the Experimental Data

Following calibration, the removal of background concentrations and the identification of the start and end times of each trace, the temporal concentration profiles at each fluorimeter were analysed. Results from injections in steady flow conditions (recorded before and after injections in unsteady flow) were compared to the values obtained by Hart et al. (2016) and showed good agreement.

The new data analysis presented here focuses on the two injections (Injections 2 and 3) made during the unsteady phase of each test. This paper presents the data recorded by all the fluorimeters to illustrate the processes. However, for quantifying longitudinal dispersion coefficients, to ensure that all the measurements analysed were obtained during the unsteady transient flow conditions, the study reach used is restricted to the 4.4 m length of pipe between fluorimeters located at 2.68 m and 7.08 m.

We first apply Equation 3, the traditional steady-state routing of temporal concentration profiles in actual time, hereafter referred to as 'temporal routing', to the study reach data. We then similarly apply Equation 6, solute routing in flow weighted time, hereafter referred to as 'flow weighted routing'. In both cases we use the previously published (Hart et al., 2016) steady state dispersion coefficient relationship, Equation 4, although for the latter converted using Equation 7. Finally, we quantify the dimensionless longitudinal dispersion coefficient and mean travel time through least-squares optimisation of Equation 6 to the measured data, producing 'optimised' values. Goodness-of-fit has been quantified using the R_t^2 correlation coefficient (Young et al., 1980). Mean values derived from five repeat tests were determined in each case, whilst the data presented in the figures is from the first of the repeat injections.

Results

Recorded Trace Data

Figures 4a & 5a show the recorded temporal concentration profiles, for accelerating flow conditions, from each of the six fully operational fluorimeters. Also plotted are the temporal variations of Reynolds number and cumulative volume, both calculated from the instantaneous flow meter output. Figure 4a shows results from Test 1 with a 5 s acceleration duration, where the flow is always turbulent. Figure 5a shows results from the early injection (2) in Test 3, performed for a 60 s acceleration, where the flow is accelerating from laminar to turbulent. Figures 4b & 5b show the temporal concentration profiles with the peak concentration values centred on zero. Under these accelerating flow conditions, the temporal concentration profiles do not show an increase in spread with distance or travel time. On the contrary, a reduction in spread with distance is observed due to

the accelerating flow conditions. Considering the concentration profiles in flow weighted time, Figures 4c & 5c, again centring the peaks at zero, show a clear, systematic increase in spread with distance from injection, in agreement with standard dispersion theory. This confirms the applicability of the flow weighted time approach.

Note that in Figures 4c and 5c, the flow weighted time was calculated using the cumulative volume for the entire test, together with the system volume of the study reach. Normally each reach would be examined with its own flow weighted time, leading to each trace being stretched/squeezed to fit a flow weighted travel time of 1. However, such a manipulation would mask the increasing spread with distance from injection.

Figure 5 shows multiple peaks in the temporal concentration profiles at all measurement locations other than for the fluorimeter at x = 0.50 m. This 'disaggregation' of the upstream single peak to multiple downstream peaks is evident in all injection 2 traces recorded in Test 3. This novel observation will be fully addressed in the Discussion section.

The time of the centroid of each temporal concentration profile has been used to characterise the flow conditions under which each of these traces was recorded. In Table 1, columns 1 & 2 summarise the test numbers and the acceleration durations, with injection number, 2 or 3, shown in column 3. Columns 4 and 5 present the values of the instantaneous Reynolds numbers at the centroid times for the upstream and downstream temporal concentration profiles at 2.68 m and 7.08 m respectively, with the temporal mean value given in column 6. Despite Test 3 commencing during laminar flow conditions, all the traces analysed through the study reach were performed with mean Reynolds numbers denoting turbulent flow. Average values for the accelerating flow tests, 1 and 3, were around 31,000, apart from injection 2 for the 60 s acceleration duration which had values of approximately 12,500. Average Reynolds numbers for the decelerating flows tests, 2 and 4, for injection 2 were around 44,750, with injection 3 having smaller values of around 25,000. Comparing flow conditions across the five repeat injections in all traces, they showed little variation; the standard deviation in Re was always $\leqslant$ 1,200, with an average standard deviation of 200.

Temporal routing

This section examines the ability of the standard steady-state temporal routing approach to predict downstream concentrations in unsteady flow conditions in actual time (Equation 3). The travel time (from tracer mean velocity) and dispersion coefficients (from Equation 4) were obtained from the equivalent mean steady flow conditions. Sample results from the first of the repeat injections for all the Tests for 5 s, 10 s and 60 s acceleration duration, with both early and late injection, are shown in Figures 6 to 9 respectively. The predicted temporal concentration profiles for 5 s, 10 s and 60 s acceleration durations are shown by the red chain dashed line for all the tests. The secondary x axis shows 10% increments of flow weighted time, to illustrate how rapidly the flow changed. The results show the measured downstream concentration profiles at 7.08 m (grey filled circles). The blue and black dashed lines in Figures 6 to 9 will be discussed in the following sections. R_t^2 values (denoted *t*) are given in the upper right corner. The mean quality of the fit of the temporal routing predictions has an R_t^2 value of 0.785.

For the majority of conditions, the predictions show that the travel time is accurately represented by the recorded tracer mean velocity. In the accelerating flow cases, Test 1 and 3, the travel time is slightly overestimated compared to the measured concentration profiles. This is a result of using the estimates of travel times based on the trace centroid Reynolds numbers. Predictions made for the different acceleration durations in decelerating flows, Tests 2 & 4, Figures 7 and 9, exhibit dispersion similar to the recorded data. This can be seen in both the spread and peak concentration, where

predicted concentration profiles are similar to the measured profiles. Under accelerating flow conditions, Tests 1 & 3, Figure 6 and 8, the predicted temporal concentration profiles exhibit greater dispersion effects than the recorded data, as shown by the greater spread, and more noticeably, in the reduced peak concentrations. Peak concentration values appear to be around 60% of the recorded concentrations for all the acceleration durations, except the late injection during the 60 s acceleration duration, Figure 6d and 8d.

Overall, these results show that temporal routing, using actual time for unsteady flow conditions, is accurate for longer acceleration durations and for decelerating flow conditions, agreeing with the results of He and Jackson (2000) and Greenblatt and Moss (2004).

Flow weighted routing

This section demonstrates the ability of solute routing in the flow weighted time domain to predict downstream concentrations in unsteady flow conditions (Equation 6). As with the temporal routing, the travel time (from tracer mean velocity) and dispersion coefficients (Equation 4) have been obtained from the equivalent mean steady flow conditions. Note the dispersion coefficients have been converted to dimensionless flow weighted time dispersion coefficients (Equation 7). The predicted flow weighted routing concentration profiles for 5 s, 10 s and 60 s acceleration durations are shown by the solid blue line in Figures 6 to 9 for all the tests. Whilst the routing has been performed in flow weighted time, for ease of comparison the results are presented in actual time. R_t^2 values (denoted ϕ) are given in the upper right corner. The quality of the fit to the data of these predictions made in flow weighted time has a mean R_t^2 value of 0.960, significantly closer to the recorded data than the predictions made using temporal routing (R_t^2 = 0.7).

Flow weighted routing travel times exhibit the same features as the temporal routing travel times, for the same rason. . In all test cases, both accelerating and decelerating flow conditions, and across all the transient times studied, the flow weighted routing predictions exhibit very good agreement with both spread and peak concentration. This improvement is most noticeable under accelerating flow conditions, Tests 1 & 3, shown clearly in Figures 6a-c and 8a-c. The benefit and accuracy of using flow weighted time to predict dispersion under time-varying flow conditions, whilst using parameters obtained from steady flow experiments, is very clearly demonstrated.

Optimised dispersion coefficients based on flow-weighted time

Dimensionless flow weighted time dispersion coefficients were fit to the laboratory data by optimisation of Equation 6. The predicted optimised flow weighted routing concentration profiles for 5 s, 10 s and 60 s acceleration durations are shown by the black dashed line in Figures 6 to 9 for all the tests. Again, whilst the routing has been performed in flow weighted time, for ease of comparison the results are presented in actual time. R_t^2 values (denoted O) are given in the upper right corner. The quality of the optimised fit to the data is very good, with an average R_t^2 value of 0.995. The worst individual value, from Test 3 for accelerating flow with the shortest 5 s acceleration duration, had an R_t^2 of 0.982, Figure 8a.

The optimised predictions are only slightly more accurate than the predictions made using Equation 4 and Equation 7. All flow weighted routing predictions are very good fits, confirming the suitability of the flow-weighted routing approach for predicting concentrations in unsteady flow conditions and the use of equivalent steady-state parameters to estimate unsteady dispersion. For most engineering applications, all these results are good representations.

Discussion

Predictions based on steady flow non-dimensional dispersion coefficients

The optimised dimensionless flow weighted time dispersion coefficients were converted to the standard dimensionless longitudinal dispersion coefficient, *D*/*ud*, and are shown in Table 1, column 10, together with the mean R_t^2 values (column 11) from the five repeat tests. Table 1 also shows the equivalent predicted steady-state dispersion coefficient in column 7 and R_t^2 values when applied using temporal routing in column 8 and flow weighted routing in column 9. This section investigates how the optimised *D*/*ud* in unsteady conditions compares to *D*/*ud* predicted using the previously published relationship for steady flow conditions, Equation 4 (Hart et al., 2016).

The mean Re over the tracer travel time (Table 1, column 6) signified fully turbulent conditions for all the current unsteady tests, and hence the predicted *D*/*ud* values show very little variation, with all values around 0.41, Table 1, column 7. It should be noted that Equation 4 was derived from the optimised longitudinal dispersion coefficient between fluorimeters located at 4.89 m and 13.05 m downstream from the injection location, a longer study reach than was possible for these unsteady flow tests.

The percentage differences between the optimised values and those predicted by Equation 4, (Hart et al., 2016) are given in Table 1, column 12. The decelerating flow conditions, Tests 2 & 4, show greater differences from the steady flow values than the accelerating flow conditions, Tests 1 & 3, with a mean difference of 40%. It is encouraging that the differences confirm the trend suggested by the results of He and Jackson (2000) and Greenblatt and Moss (2004), in that the influence of unsteady conditions reduces with increasing acceleration duration. That is, the slower the flow changes, the more reliably longitudinal dispersion can be approximated to the steady-state values.

The decelerating flow results, Tests 2 & 4, show that all the optimised values of *D*/*Ud* obtained from the unsteady flow conditions are less, almost half the value of those obtained from the equivalent steady flow tests. Under accelerating flow conditions, Tests 1 and 3, the average percentage difference between the analysed optimised values and those predicted by Hart et al. (2016) (Table 1, column 12) is approximately zero, with values under predicted for 5 s and 10 s acceleration durations and over predicted for 60 s acceleration duration. Possible reasons for these observed discrepancies are explored in the next subsection.

Limitations of the temporal routing approach

Under decelerating conditions all the values of Optimised *D*/*ud* are less than those obtained from the equivalent steady flow tests. It is hypothesised that the lower values are a result of a low turbulence dissipation rate. This leads to residual turbulent fluctuations in the flow after steady mean velocity has been achieved. These residual turbulent fluctuations would generate greater cross-sectional mixing, compared to the level expected for the same steady turbulent flow conditions. This would reduce the effect of differential longitudinal advection, reducing the magnitude of the longitudinal dispersion coefficient.

Under accelerating flow conditions the average percentage difference between the analysed optimised values and those predicted by Hart et al. (2016) is small. The higher percentage differences are probably due to a greater influence of dispersion at the low initial Reynolds number. Results from the steady flow test cases confirm increased values of *D*/*ud* as Re reduces. This is further supported by the trend in the percentage differences, from larger positive to larger negative differences as acceleration duration increases.

Multiple peaks

During the initial investigation, temporal concentration profiles with multiple peaks were recorded at the fluorimeter 2.68 m downstream from the injection, as shown in Figure 5a and at all subsequent fluorimeters. These were consistently observed in every trace during the acceleration from initial laminar flow conditions, Test 3. To check whether this was an artefact of the experimental set-up, such as a limitation of the injection system, data from the fluorimeter 0.5 m downstream from the injection was used. Despite the fluorimeter being unable to record the peak concentration, the data shown in Figure 5a confirms the shape of the concentration profile immediately after injection. This clearly shows a single peak, almost symmetrical, with the peak concentration greater than the maximum recordable concentration. Similar concentration profiles were recorded for all the Injection 2 traces conducted in Test 3.

Two examples of the concentration profiles with multiple peaks caused by disaggregation of the tracer cloud in Test 3, recorded 2.68 m downstream from the injection, are shown in Figure 10 (grey dots). Figure 10a shows the trace for the shortest acceleration duration, whilst Figure 10b shows the trace for Injection 3 under the 60 s acceleration duration. For this example, travel times from the upstream fluorimeter 0.50 m downstream from the injection, a single peak, to each of the multiple peaks recorded 2.68 m are approximately 7, 10 and 16 s. These are over a distance of 2.18 m, under significantly accelerating flow, as shown by the 10 % increments of flow weighted time. If cross-sectionally well-mixed, this suggests that approximately 5 % of the tracer arrives with a mean velocity of 0.31 m/s, with the majority of tracer, 85 %, travelling at 0.22 m/s and a third discrete pulse, approximately 10 % at 0.14 m/s. The 100 % difference in flow velocity between individual pulses, is similar in magnitude to the spatial differences in velocity recorded by Kurokawa and Morikawa (1986).

Assuming that the tracer is cross-sectionally well-mixed in the pipe during the initial laminar flow as the flow is accelerated, the tracer in the centre of the pipe is accelerated more rapidly than the tracer near the pipe boundary. If the flow remains laminar there would be little radial exchange. This acceleration leads to an exaggerated version of the process that creates highly skewed concentration profiles in steady laminar flow, to the point where the dye cloud actually disaggregates. This hypothesis is supported by Kurokawa and Morikawa (1986), whose velocity profiles in Figure 1 show a significant difference between centreline and boundary region velocities prior to the creation of fully turbulent conditions. It is suggested that the multiple peaked tracer profiles are a result of this observed effect. Within the scope of this study, velocity measurements to support this hypothesis were not available and further work is required to fully elucidate the processes.

To illustrate the limitations of routing predictions when this disaggregation occurs, the same routing analysis was performed for the data in Figure 10 using a Gaussian distribution fitted to the data recorded at the fluorimeter at 0.5 m for the upstream temporal concentration profile to avoid the problem with off-scale data. The results for data analysis optimised in flow weighted time (black dashed), predictions routed in actual time (red chain dashed), and in flow weighted time (solid blue) are shown. Hart et al. (2016) showed the limitations of employing a Gaussian routing approach for laminar flows and these predictions illustrate similar, although different, concerns. The actual time routed predictions (red chain dashed line) significantly over estimate the longitudinal dispersion, with very low R_t^2 values. The flow weighted time routing predictions are better, but since the upstream concentration profile has a single peak, the ADE-based routing cannot reproduce the recorded multiple peaks, as it does not represent the disaggregation process. This highlights the need for further investigations to explain the cause of the disaggregation during laminar to turbulent

flow accelerations. It also illustrates the need to understand the physical processes occurring during low Re flow accelerations in order to make realistic predictions of mixing under these conditions in pipe networks.

Conclusions

Experimental studies of longitudinal dispersion in unsteady flows in pipes have been conducted and analysed with the resulting dispersion coefficients compared to those obtained in previous work on steady flows. The analysis has shown the limitations of employing a steady-state routing approach and confirmed that the ability of this method to describe observations decreases with increasing rates of change of discharge. However, employing a routing approach based on the flow weighted time significantly improved predictions for the acceleration durations studied, even when coefficients derived from steady flow experiments are employed in the routing. In practice this means that it is feasible to apply coefficients derived from steady flow experiments within modelling tools, provided that flow-weighted time is adopted in the routing process.

From the experiments undertaken in both turbulent to turbulent and laminar to turbulent flows, the results show that smaller values of the longitudinal dispersion coefficient, when compared to the equivalent steady flow conditions, were obtained during decelerating flow. It is suggested that this is a result of residual turbulence in the flow.

During acceleration from laminar to turbulent flows a novel disaggregation of the tracer cloud was observed. This occurred during the initial acceleration, and the resulting multiple peaked profiles were recorded at all the locations along the pipe. It is recommended that further detailed studies, including measurements of temporal variations in the velocity and tracer cloud distributions across the pipe, should be undertaken to elucidate and quantify the specific processes that lead to this previously unreported phenomenon.

Data Availability Statement

The data, models, and code generated or used during the study are available in a repository online in accordance with funder data retention policies, see Hart et al (2021), https://doi.org/10.15131/shef.data.14135591

Acknowledgements

Many thanks go to Mr Ian Baylis who provided the technical support for all the laboratory studies conducted at the University of Warwick. This work was supported by the EPSRC Grant EP/P012027/1.

Notation

The following symbols are used in this paper:

A	=	cross-sectional area;
c	=	concentration;
$c(x,t)$	=	concentration at location x at time t;
D	=	longitudinal mixing coefficient;
D_m	=	molecular diffusion coefficient;
J	=	flow weighted time longitudinal dispersion coefficient;
M	=	mass of contaminant;
Q	=	flow rate;
Re	=	Reynolds number;
R_t^2	=	correlation coefficient;

r = pipe radius;
$S(x,\gamma)$ = concentration at location x at flow weighted time γ;
s = distance between measurement points;
t = time;
$\bar{t}$ = travel time;
u = velocity;
V = system volume;
x = longitudinal distance;
Γ = distance from the pipe wall;
γ = integration variable;
ϕ = non-dimensional flow weighted time;

Subscripts

i = initial;
f = final

References

Basha, H.A. and Malaeb, L.N. (2007) Eulerian–Lagrangian Method for Constituent Transport in Water Distribution Networks. *Journal of Hydraulic Engineering*, ASCE, 133(10), 1155-1166.

Buchberger, S.G.; Carter, J.T.; Lee, Y., and Schade, T.G. (2003). Random demands, travel times and water quality in deadends. American Water Works Association Research Foundation, Report 90963F:470, 2003.

Chatwin, P.C. (1970) Approach to normality of concentration distribution of a solute in a solvent flowing along a straight pipe. *Journal of Fluid Mechanics*, 43, 321–352. https://doi.org/10.1017/S0022112070002409

Danckwerts, P. V. (1953). Continuous flow systems distribution of residence times. *Chemical Engineering Science*, 2(1), 1–13. https://doi.org/10.1016/0009-2509(53)80001-1

Fernandez-Sempere, J., Font-Montesinos, R., & Espejo-Alcaraz, O. (1995). Residence time distribution for unsteady-state systems. *Chemical Engineering Science*, 50(2), 223–230. https://doi.org/10.1016/0009-2509(94)00230-O

Fischer, H.B., List, J.E., Koh, C. R., Imberger, J., & Brooks, N. H. (1979). *Mixing in Inland and Coastal Waters*. Elsevier.

Greenblatt, D. & Moss, E.A. (2004). Rapid temporal acceleration of a turbulent pipe flow. *Journal of Fluid Mechanics*, 514, 65–75. https://doi.org/10.1017/S0022112004000114

Hart, J., Guymer, I., Jones, A.E. & Stovin, V.R. (2013). Longitudinal Dispersion Coefficients within Turbulent and Transitional Pipe Flow. In P. Rowinski (ed.), Experimental and Computational Solutions of Hydraulic Problems, GeoPlanet: Earth and Planetary Sciences, https://doi.org/10.1007/978-3-642-30209-1_28, Springer-Verlag Berlin Heidelberg 2013.

Hart, J., Guymer, I., Sonnenwald, F., & Stovin, V. (2016). Residence time distributions for turbulent, critical, and laminar pipe flow. *Journal of Hydraulic Engineering*, 142(9), 04016024. https://doi.org/10.1061/(ASCE)HY.1943-7900.0001146

Hart, J., Sonnenwald, F., Guymer, I. (2021). "Temporal Concentration Profiles in Steady and Unsteady Pipe Flow. V1." The University of Sheffield Online Research Data. https://doi.org/10.15131/shef.data.14135591

He, S. and Jackson, J.D. (2000). A study of turbulence under conditions of transient flow in a pipe. *Journal of Fluid Mechanics*, 408:1-38. https://doi.org/10.1017/S0022112099007016

Holland, J. F., Martin, J. F., Granata, T., Bouchard, V., Quigley, M., & Brown, L. (2004). Effects of wetland depth and flow rate on residence time distribution characteristics. *Ecological Engineering*, 23(3), 189–203. https://doi.org/10.1016/j.ecoleng.2004.09.003

526 Kurokawa, J. and Morikawa, M. (1986) Accelerated and decelerated flows in a circular pipe. The
527 Japan Society of Mechanical Engineers, 29(249), 758-765.
528 https://doi.org/10.1299/jsme1958.29.758
529 Leclerc, J., Claudel, S., Lintz, H., Potier, O., & Antoine, B. (2000). Theoretical interpretation of
530 residence-time distribution measurements in industrial processes. *Oil & Gas Science and*
531 *Technology*, 55(2), 159–169. https://doi.org/10.2516/ogst:2000009
532 Levenspiel, O. (1972). *Chemical Reaction Engineering*. John Wiley & Son, Inc.
533 Nauman, E. (1969). Residence time distribution theory for unsteady stirred tank reactors. *Chemical*
534 *Engineering Science*, 24(9), 1461–1470. https://doi.org/10.1016/0009-2509(69)85074-8
535 Romero-Gomez, P. and Choi, C.Y. (2011). Axial Dispersion Coefficients in Laminar Flows of Water-
536 Distribution Systems. *Journal of Hydraulic Engineering*, ASCE, 137(11), 1500-1508.
537 https://doi.org/10.1061/(ASCE)HY.1943-7900.0000432
538 Piazza, S., Blokker E.J.M., Freni, G., Puleo, V. and Sambito, M. (2020). Impact of diffusion and
539 dispersion of contaminants in water distribution networks modelling and monitoring. *Water*
540 *Supply*, 20 (1): 46–58.
541 Taylor, G. I. (1953). Dispersion of soluble matter in solvent flowing slowly through a tube
542 *Proceedings of the Royal Society,* 219(1137), 186–203.
543 https://doi.org/10.1098/rspa.1953.0139
544 Taylor, G. I. (1954) The dispersion of matter in turbulent flow through a pipe. *Proc. R. Soc.*,
545 223(1155), 446–468. https://doi.org/10.1098/rspa.1954.0130
546 Wahl, M. D., Brown, L.C., Soboyejo, A.O., & Dong, B. (2012). Quantifying the hydraulic performance
547 of treatment wetlands using reliability functions. *Ecological Engineering*, 47, 120–125.
548 https://doi.org/10.1016/j.ecoleng.2012.06.009
549 Werner, T.M. & Kadlec, R.H. (1996). Application of residence time distributions to stormwater
550 treatment systems. *Ecological Engineering*, 7(3), 213–234. https://doi.org/10.1016/0925-
551 8574(96)00013-4
552 Young, P., Jakeman, A., & McMurtrie, R. (1980). An instrumental variable method for model order
553 identification. *Automatica*, *16*(3), 281–294. https://doi.org/10.1016/0005-1098(80)90037-0
554
555

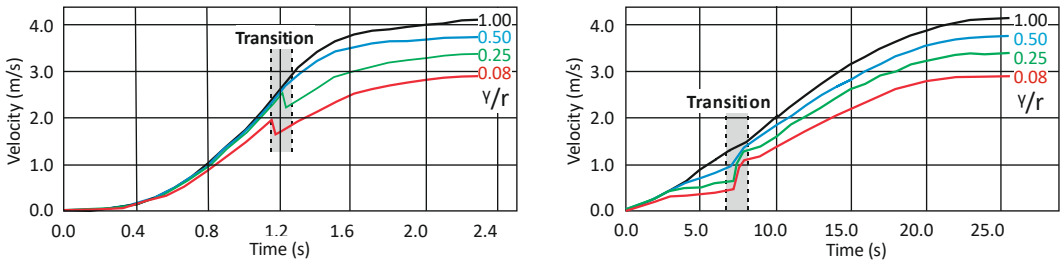

Figure 1 – Temporal variations in velocity for accelerated flows in pipes (reproduced from Kurokawa and Morikawa, 1986, Fig. 5, with permission from The Japan Society of Mechanical Engineers) for acceleration duration a) 2.5 s and b) 25 s.

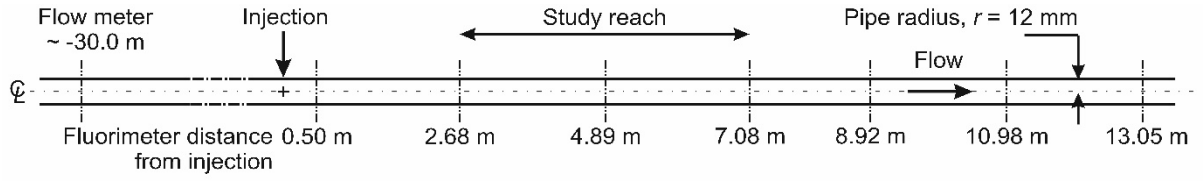

Figure 2 – Laboratory configuration

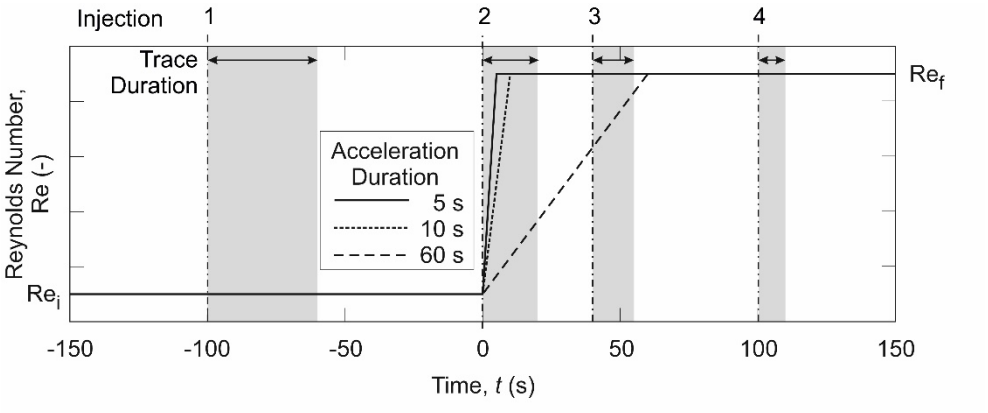

Figure 3 – Schematic of flow conditions, grey shaded area indicates duration of trace
Note: Re_f may be less than Re_i

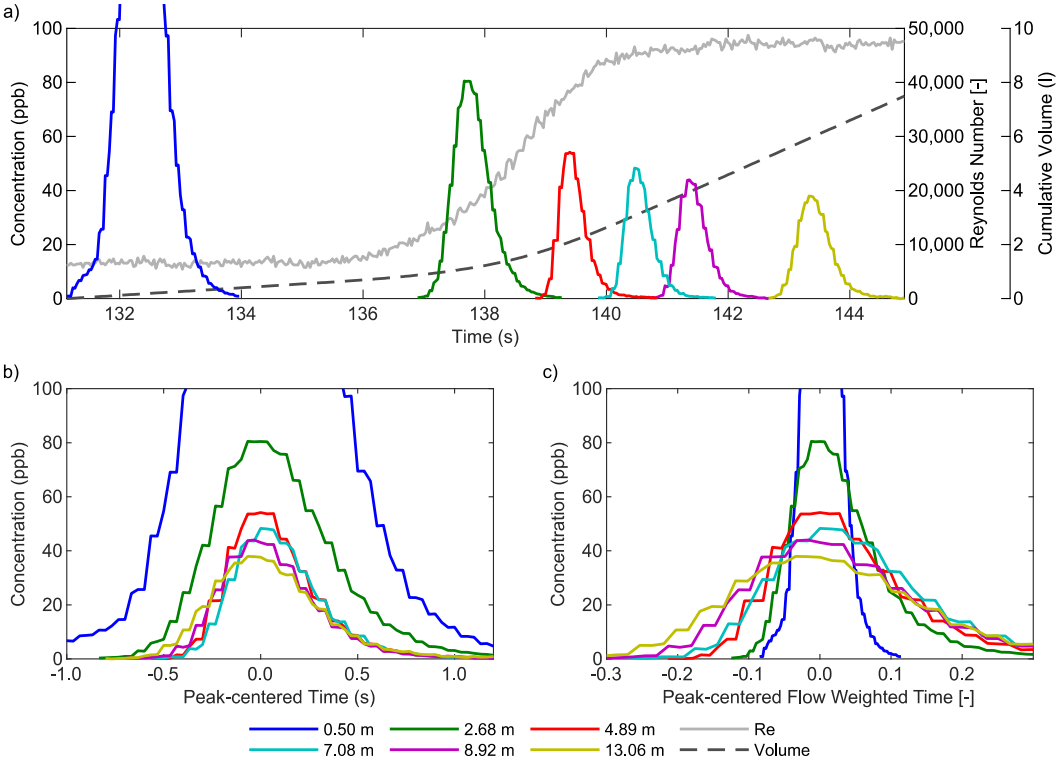

570

571 Figure 4 Test 1 with 5 s Acceleration duration: a) temporal variation of measured concentrations, Re
572 and cumulative volume; and peak centred concentrations in b) actual time and c) flow weighted
573 time.

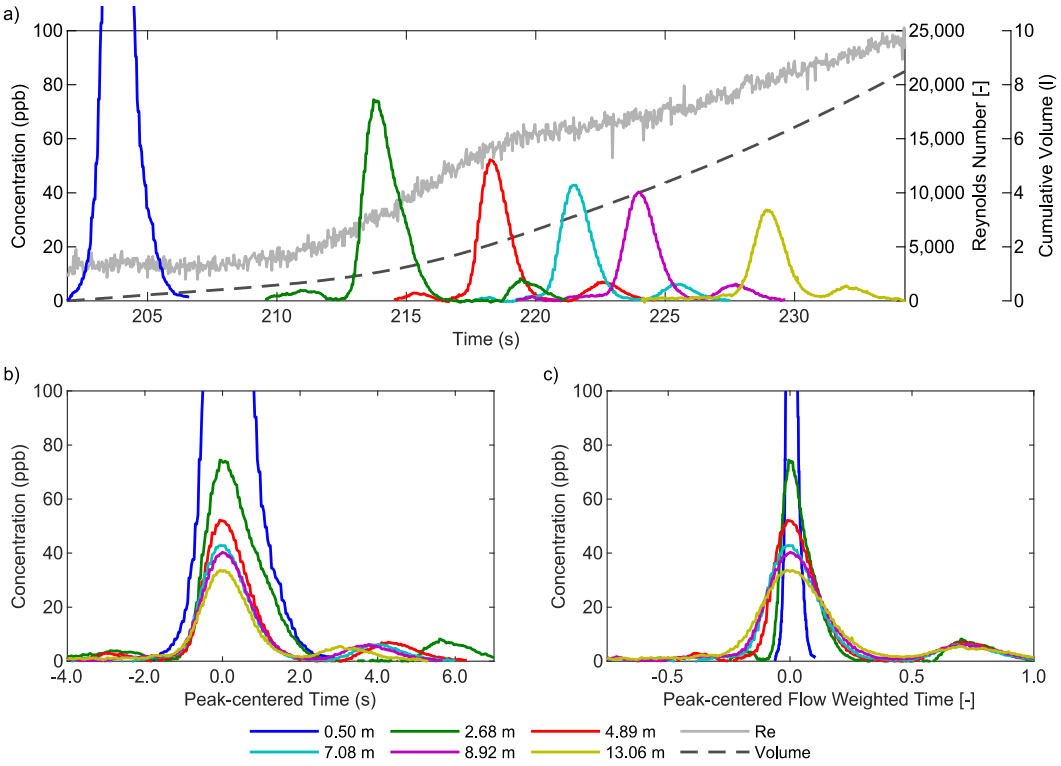

574

575 Figure 5 Test 3 with 60 s Acceleration duration: a) temporal variation of measured concentrations,
576 Re and cumulative volume; and peak centred concentrations in b) actual time and c) flow weighted
577 time.

578

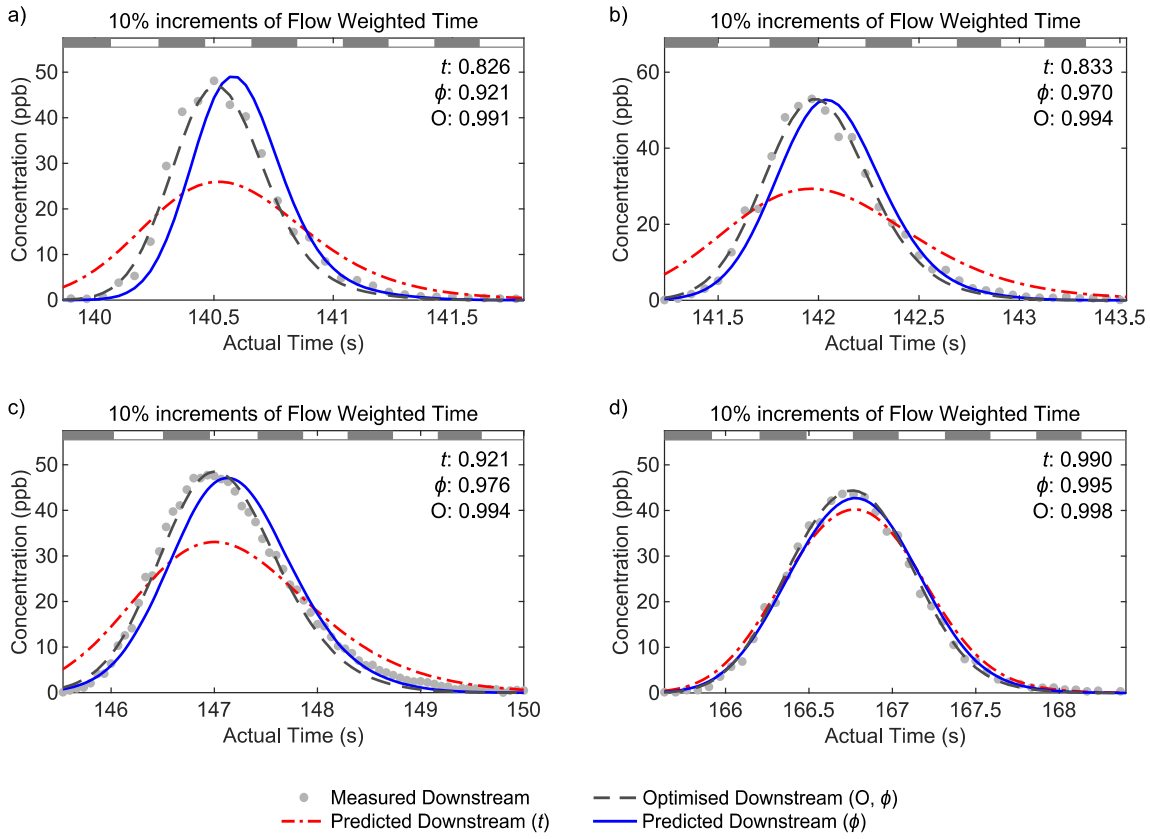

Figure 6 – Test 1: Measured data; Optimised analysis (O) and predicted downstream concentration profiles for a) 5 s, b) 10 s, c) 60 s acceleration duration injection 2, and d) 60 s acceleration duration injection 3. Routing predictions, assuming mean dispersion coefficient, based on Actual Time, (t) and Flow Weighted Time, (ϕ), with R_t^2 shown in the upper right corner.

579

580

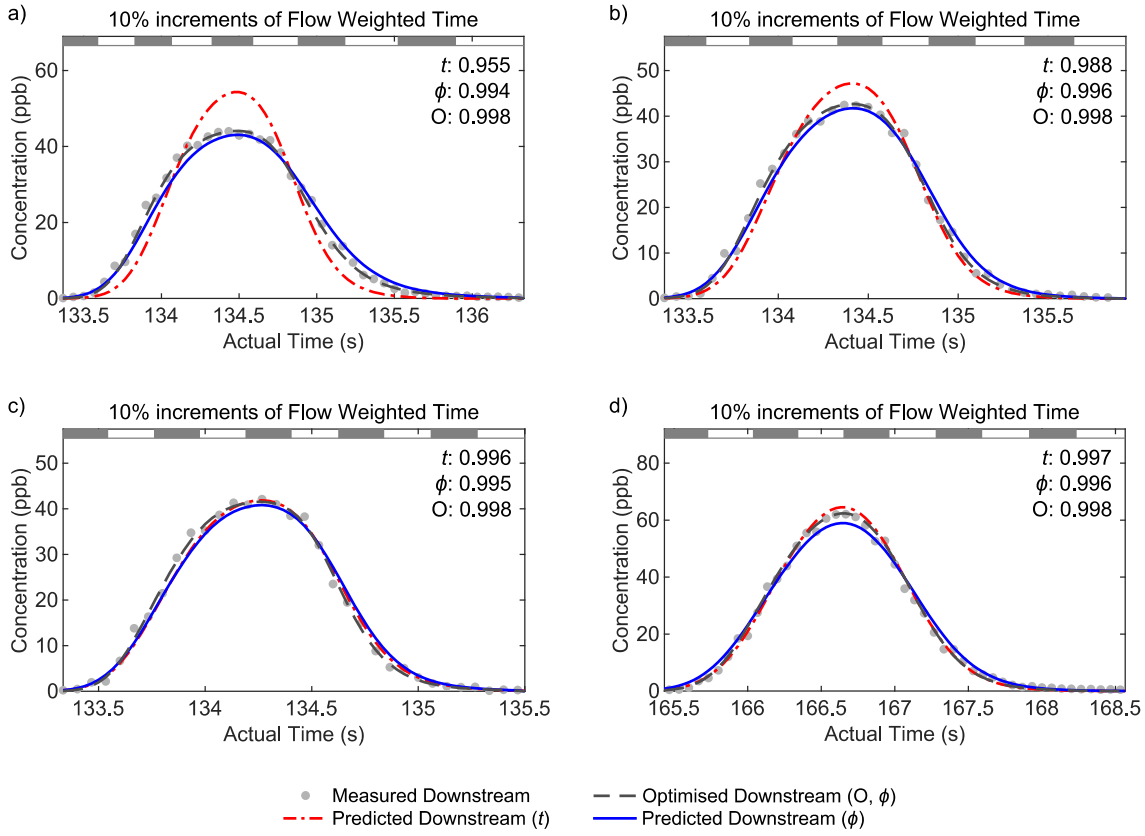

Figure 7 – Test 2: Measured data; Optimised analysis (O) and predicted downstream concentration profiles for a) 5 s, b) 10 s, c) 60 s acceleration duration injection 2, and d) 60 s acceleration duration injection 3. Routing predictions, assuming mean dispersion coefficient, based on Actual Time, (t) and Flow Weighted Time, (ϕ), with R_t^2 shown in the upper right corner.

581
582

583

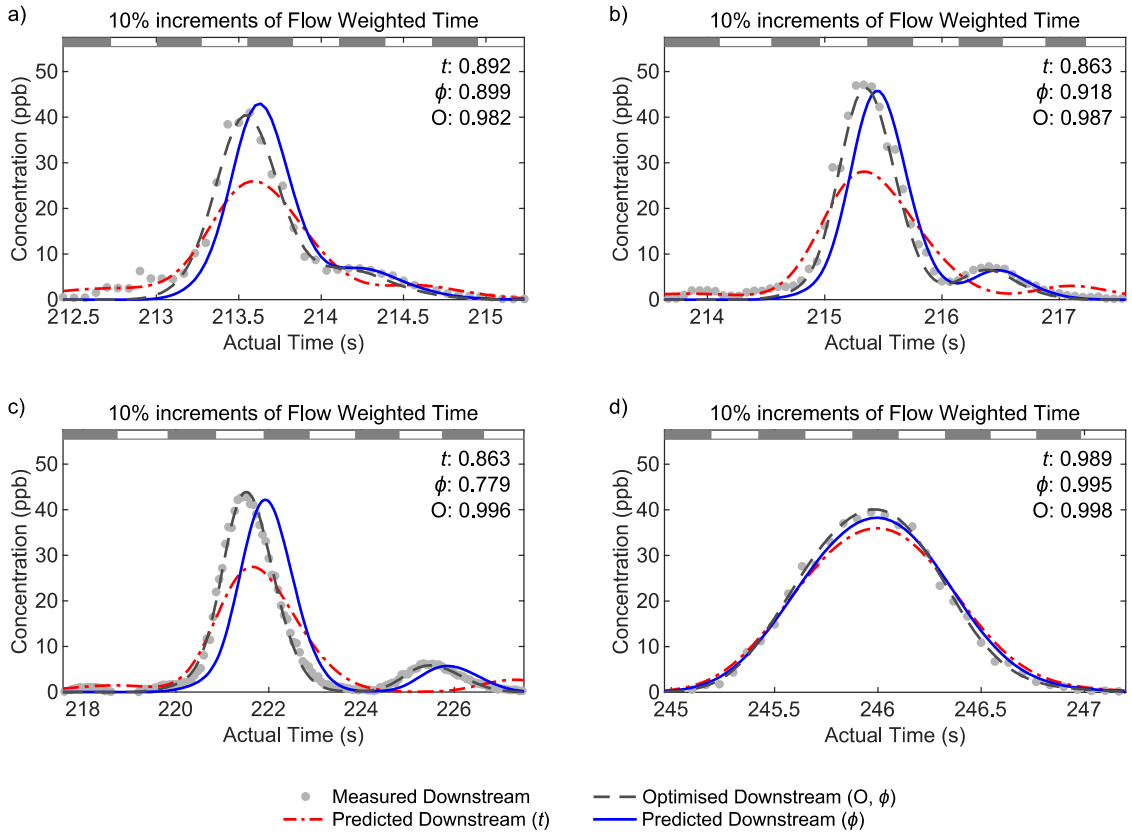

Figure 8 – Test 3: Measured data; Optimised analysis (O) and predicted downstream concentration profiles for a) 5 s, b) 10 s, c) 60 s acceleration duration injection 2, and d) 60 s acceleration duration injection 3. Routing predictions, assuming mean dispersion coefficient, based on Actual Time, (t) and Flow Weighted Time, (ϕ), with R_t^2 shown in the upper right corner.

584
585

586

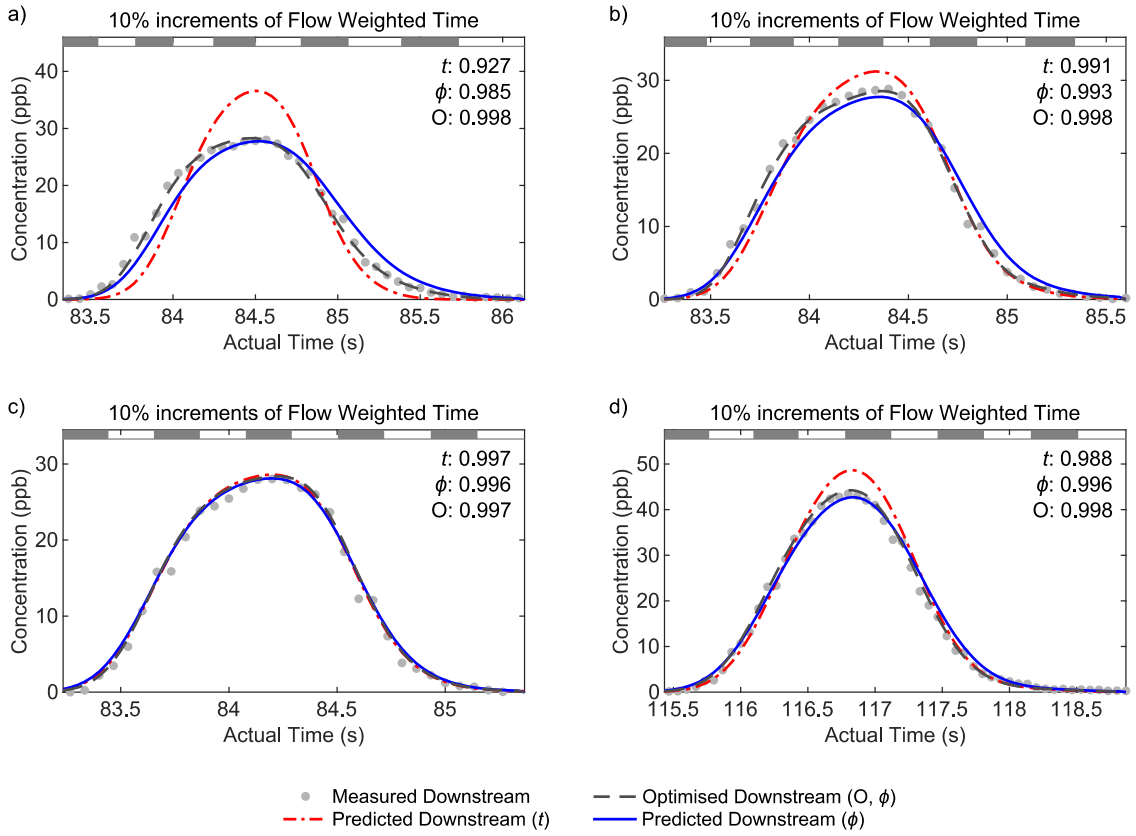

Figure 9 – Test 4: Measured data; Optimised analysis (O) and predicted downstream concentration profiles for a) 5 s, b) 10 s, c) 60 s acceleration duration injection 2, and d) 60 s acceleration duration injection 3. Routing predictions, assuming mean dispersion coefficient, based on Actual Time, (t) and Flow Weighted Time, (ϕ), with R_t^2 shown in the upper right corner.

587

588

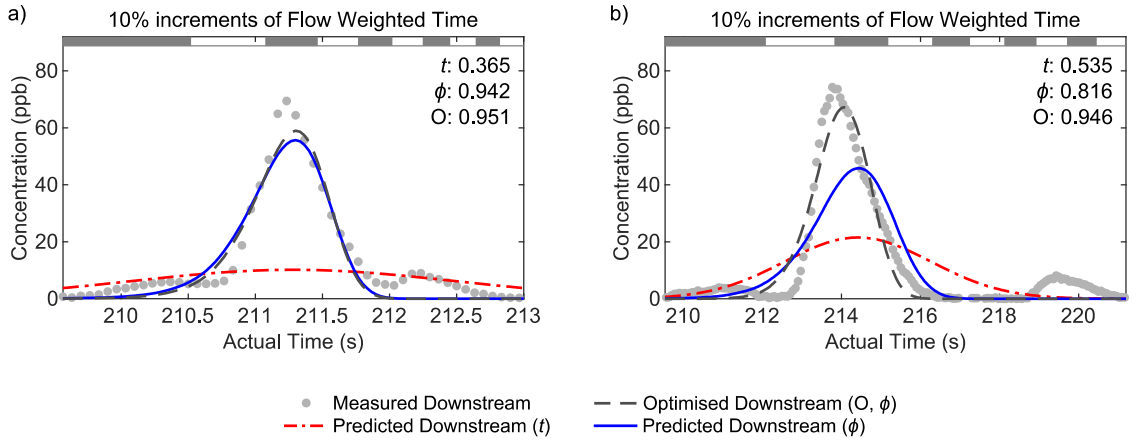

Figure 10 – Test 3 for acceleration from laminar to turbulent flow: Measured data; Optimised analysis (O) and predicted downstream concentration profiles between 0.5 m and 2.68 m for a) 5 s and b) 60 s acceleration duration. Routing predictions, assuming mean dispersion coefficient, based on Actual Time, (t) and Flow Weighted Time, (ϕ), with R_t^2 shown in the upper right corner.

589

590 Table 1 – Details of Experimental Runs

Test	Acceleration duration (s)	Injection	Trace[1] Reynolds Number			Predicted from Equation 4 (Hart et al., 2016)			Optimised Flow Weighted Routing		Diff. (%) $\Delta(D/ud)$
			2.68 m	7.08 m	Mean	D/ud	R_t^2 Temporal Routing (t)	R_t^2 Flow Weighted Routing (ϕ)	D/ud	R_t^2	
1	5	2	18,600	45,700	34,900	0.42	0.211	0.931	0.49	0.991	17
	10	2	14,200	32,600	23,600	0.42	0.284	0.964	0.43	0.994	2
	60	2	8,600	15,200	12,000	0.48	0.710	0.969	0.44	0.994	-8
	60	3	25,900	28,200	27,100	0.42	0.988	0.995	0.32	0.998	-24
2	5	2	46,300	35,800	42,400	0.41	0.943	0.992	0.23	0.998	-44
	10	2	46,500	40,400	43,900	0.41	0.981	0.996	0.23	0.998	-44
	60	2	46,800	45,400	46,200	0.41	0.996	0.996	0.25	0.998	-39
	60	3	27,600	25,500	26,500	0.42	0.992	0.996	0.27	0.998	-36
3	5	2	22,900	49,000	41,300	0.41	0.479	0.817	0.55	0.982	34
	10	2	16,700	35,400	27,800	0.42	0.503	0.930	0.43	0.991	2
	60	2	8,300	16,000	13,300	0.47	0.573	0.806	0.43	0.994	-9
	60	3	30,300	32,200	31,200	0.42	0.991	0.996	0.29	0.998	-31
4	5	2	46,900	36,300	42,800	0.41	0.938	0.987	0.21	0.998	-49
	10	2	47,300	41,300	44,700	0.41	0.982	0.994	0.22	0.998	-46
	60	2	47,300	46,400	46,800	0.41	0.997	0.997	0.29	0.998	-29
	60	3	27,100	24,100	25,500	0.42	0.992	0.996	0.30	0.998	-29
				Mean			0.785	0.960		0.995	
				Standard deviation for repeat traces	≤ 500	< 0.001	≤ 0.057	≤ 0.064	≤ 0.07	≤ 0.004	

591 Test 1 = turbulent to turbulent accelerating flow; Test 2 = turbulent to turbulent decelerating flow

592 Test 3 = laminar to turbulent accelerating flow; Test 4 = turbulent to laminar decelerating flow.

593 [1] Taken from the centroid of temporal concentration profiles at 2.68 m & 7.08 m.